 doi:10.20944/preprints202209.0274.v2

Article

Durability Assessment Method of Hollow Thin-Walled Bridge Piers under Rockfall Impact Based on Damage Response Surface

Fei Li[1, 2, *], Yikang Liu[3], Jian Yang[3]

1 College of Civil Engineering, Longdong University, Qingyang 745000, China; lifei@ldxy.edu.cn (F.L.)
2 Provincial Key Laboratory of Engineering Properties and Applications of Loess in Colleges and Universities of Gansu Province, Gansu 745000, China
3 School of Civil Engineering, Central South University, Changsha 410075, China; liuyikang_csu@csu.edu.cn (Y.L.); yangjian_2022@163.com (J.Y.)
* Correspondence: lifei@ldxy.edu.cn

Abstract: Continuous rigid frame bridges across valleys are often at the risk of rockfalls caused by heavy rainfalls, earthquakes and debris flows in a mountainous country. Hollow thin-walled bridge piers (HTWBP) in valleys are exposed to the threat of the impact of accidental rockfalls. In the current research, ANSYS/LS-DYNA is used to establish a high-precision rockfall-HTWBP model. The rockfall-HTWBP model is verified against a scaled impact test of a previous research. A mesh independence test is also performed to obtained an appropriate mesh size. Based on the rockfall-HTWBP model, the impact force, damage and dynamic response characteristics of HTWBP under the rockfall impact are studied. In addition, a damage assessment criteria is proposed based on the response surface model combined with Central Composite Design method and Box-Behnken Design method. The main conclusions are as follows: 1）The impact force of rockfall has a substantial impulse characteristic, and the duration of the impulse load is approximately 0.01s. 2）The impacted surface of the pier is dominated by the final elliptic damage with the conical and strip damage areas as the symmetry axis. The cross-sectional damage mode is compression failure in the impact area and shear failure at the corner. 3）The maximum displacement occurs in the middle height of the pier. The maximum displacement increases with impact height, impact velocity and rockfall diameter and decreases with the uniaxial compressive strength of the concrete. 4) The initial impact velocity and diameter of the rockfall are the most significant parameters affecting the damage indices. In addition, a damage assessment method with a damage zoning diagram based on the response surface method is established for the fast assessment of the damage level of impacted HTWBP.

Keywords: rockfall impact; impact resistance; hollow thin-walled bridge pier; response surface model; durability assessment

1 Introduction

China is a mountainous country. With the continuous improvement of transportation infrastructure construction, the number of large-span bridges across valleys gradually increased. Owing to the complex terrain and extreme weather in mountain valleys, bridges across valleys are often at the risk of rockfalls caused by heavy rainfall, earthquakes and debris flows [1, 2]. Being impacted by rockfalls is not uncommon for bridges. For example, in Wenchuan County, Sichuan Province of China, due to the seismic action and days of heavy rain, a bridge pier was impacted by rockfalls, causing its collapse. In the accident, the national highway was interrupted, three people were killed and seven vehicles were damaged. Figure 1 shows the field photo of the bridge pier impacted by rockfall [1]. Continuous rigid frame bridge is an important transportation infrastructure across the valleys. The pier is generally designed as hollow thin-walled high pier

 doi:10.20944/preprints202209.0274.v2

(HTWBP) to save materials and reduce costs. HTWBPs in valleys are exposed to the threat of the impact of accidental rockfalls.

Given the high cost of full-scale test, only a few scholars have conducted full-scale test on the impact resistance of bridge piers. Consolazio et al. used a combination of full-scale ship impact test and numerical analysis to quantify the impact load, pier response, and soil response during barge–pier collision [3]. Buth et al. conducted two collisions between a truck-type tractor-trailer weighing 80,000 pounds and a full-length bridge pier at an impact speed of 80 km/h [4]. In the first test, a frontal collision between the vehicle and the bridge pier was performed, and in the second test, an eccentric distance between the vehicle and the bridge pier was observed. Compared with full-scale tests, numerical simulation is more popular in the research of impact resistance of bridge piers under rockfall impacts [5-7]. For example, Bertrand et al. analysed the reliability of reinforced concrete members under rockfall impacts and proposed a simply supported reinforced concrete member model considering material nonlinearity and contact nonlinearity [8]. Ventura et al. studied the local structural dynamic response of steel members under the impact of rockfalls [9]. A new flexible contact model was proposed for the interaction between target body and impact body. Zhang et al. studied impact force, the dynamic response of the bridge and the deformation of the track structure when collision happens between rockfall and bridge pier [10]. In addition, rockfall and vehicle collision problems have some similarities. Many researchers tried to understand the impact performance of bridge piers under vehicle impacts [11-14]. However, the main research object of the above studies is the solid concrete pier, and the rockfall impact resistance of the HTWBP has not been reported. Considering the wide engineering application of HTWBP in China, investigating the impact resistance of HTWBP under rockfall loads is greatly necessary.

Figure 1. Bridges impacted by rockfalls.

When the bridge pier is impacted by rockfalls, the impact effect damages the bridge pier. The pier is the main supporting and force transmission component of a bridge. The rockfall impact to bridge piers may lead to the collapse of the bridge, resulting in immeasurable serious consequences. Therefore, evaluating the damage of bridge pier after rockfall impacts has practical importance. Commonly used damage assessment criteria include maximum displacement criterion, residual bearing capacity criterion and maximum bearing angle criterion [15, 16]. The maximum displacement criterion and the maximum bearing angle criterion usually assume that the pier is mainly affected by bending or shear damage, whereas the residual bearing capacity criterion mainly considers the axial bearing capacity decay of the pier. However, due to the large differences in the height, diameter, strength and other characteristics of different impacted piers, the velocity and stiffness of the impactor and the strong randomness of the impact position, the impacted pier usually presents a mixed damage mode consisting of bending, shear and local compression. Therefore, a damage assessment criterion considering the mixed damage of bridge pier, which is convenient for accurate, fast assessment of bridge pier damage, needs to be proposed.

 doi:10.20944/preprints202209.0274.v2

In the current paper, ANSYS/LS-DYNA is used to establish a high-precision rockfall-HTWBP model, which is verified by drop weight test. Then, the impact force, damage and dynamic response characteristics of HTWBP under rockfall impact are studied. Finally, a damage assessment method with a damage zoning diagram based on the response surface method is established.

2 Rockfall-HTWBP impact model

2.1 FE model of bridge and rockfall

A 72+120+120+72 m continuous rigid frame bridge on the highway from Longshan to Yongshun in Hunan Province, China is taken as the research object. This bridge is chosen as the object for two reasons: (1) This bridge is located in southern China, i.e., a mountainous region where rockfall diseases frequently happen; (2) Continuous rigid frame bridges with the highest pier height of approximately 100 m are normally chosen as the research prototype [24, 25]. The bridge layout is shown in Figure 2. The cross-section of the bridge pier is a single box and single chamber section. The superstructure of the bridge is supported by HTWBPs where the middle pier is 100 m high, and the side pier is 80 m high. Based on the continuous rigid frame bridge, a geometric model is established by using HyperMesh programme, as shown in Figure 3. The size of rockfall is widely distributed. As reported by a previous study [1], the diameter of rockfalls is normally 1.5 m to 2.5 m, and three rockfall models with different diameters, i.e., 1.5 m, 2.0 m and 2.5 m are established in this research.

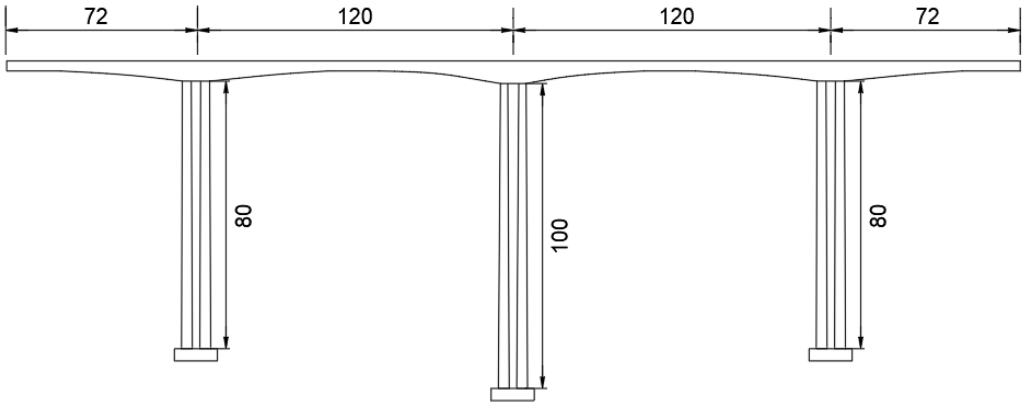

Figure 2. Layout of the bridge. (Unit: m)

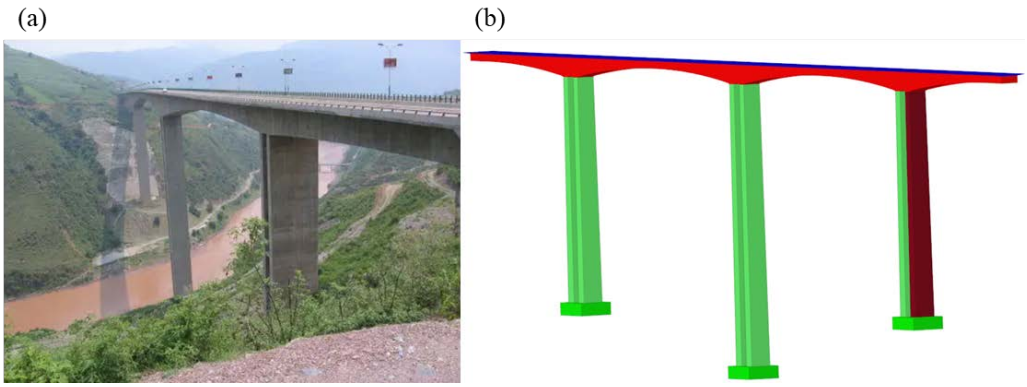

Figure 3. Geometry of the bridge: (a) Actual picture; (b) Geometry model.

After the geometric model is established, HyperMesh program is utilized to mesh the model. The bridge pier, cap and superstructure are simulated using the Solid element, which is an eight-

Preprints (www.preprints.org) | NOT PEER-REVIEWED | Posted: 20 September 2022 doi:10.20944/preprints202209.0274.v2

node element with one integral point. The longitudinal and transverse reinforcements in the pier are simulated using the Hughes-Liu beam element with one integral point. The concrete is assumed to be fully bonded to the reinforcements, implemented by the keyword *CONSTRAINED_LAGRANGE_IN_SOLID [5, 17]. The effect of the superstructure is considered by using the keyword *LOAD_BODY_Z. *CONTROL_DYNAMIC_RELAXATION with convergence factor of 0.0001 is adopted to achieve static equilibrium before impact. To improve the calculation efficiency, the grid of the impacted bridge pier is encrypted with grid size of 50 mm. The grid size of other piers is 100 mm, and the grid size of reinforcements in the pier is 100 mm. The grid size of the bridge superstructure and pier cap are 300 and 200 mm, respectively. The reinforcement is composed of 26 longitudinal reinforcement bars with a diameter of 30 mm and transverse reinforcement bars with a diameter of 16 mm and a spacing of 150 mm. The element types used for each component of the bridge and the dimensions of the grid are summarized in Table 1. The detailed finite element (FE) model of the bridge is shown in Figure 4(a). The total grid number of the rock-HTWBP model is approximately 8000000. Considering the pile-soil interaction has limited influence on the impact resistance of the bridge, the bottom of the cap is set as a fixed boundary without considering the effect of pile and soil [1]. The impact between the rockfall and HTWBP is achieved by the automatic surface-surface contact (*AUTO_CONTACT_SURFACE_TO_SURFACE).

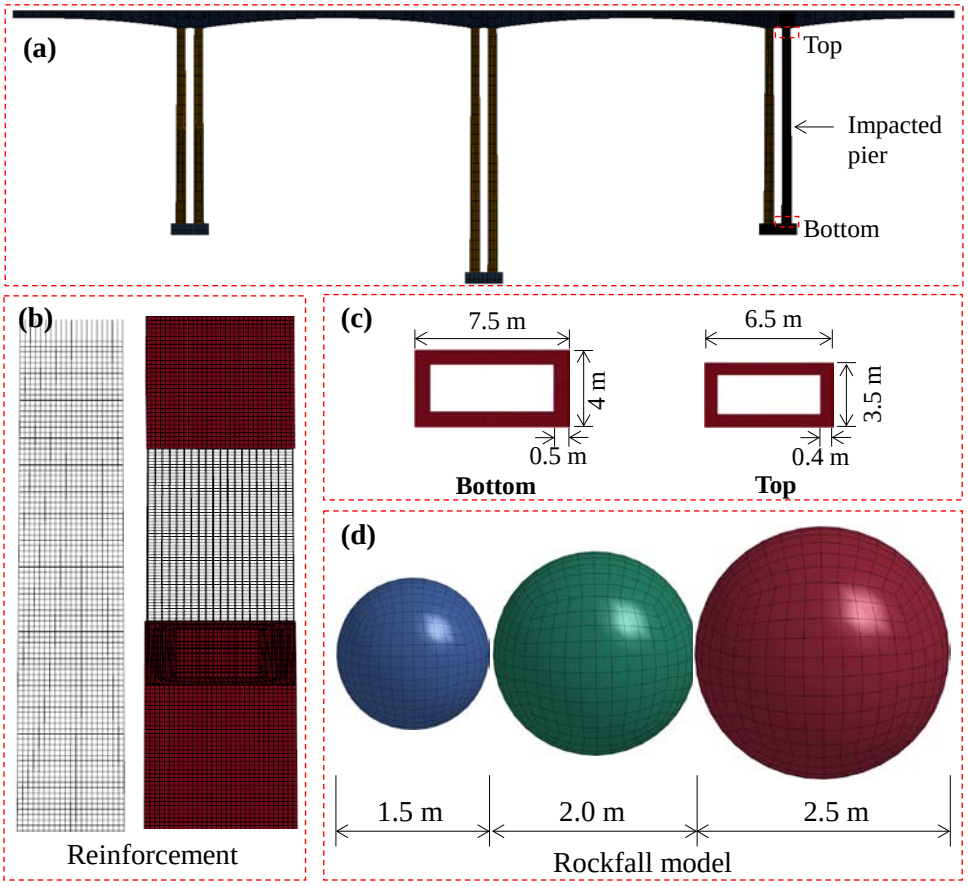

Figure 4. FE model of the bridge and rockfall.

Table 1. Element types and grid sizes.

Component	Element type	Grid size (mm)
Impacted pier	Solid	50
Other piers	Solid	100
Pile cap	Solid	200

2.2 Material model

LS-DYNA software provides a variety of material models for concrete materials [18]. The most commonly constitutive models used to simulate concrete materials in engineering applications are as follows: MAT_111 (Johnson Holmquist concrete model), MAT_72R3 (concrete damage REL3 model), MAT_96 (concrete brittle damage model), MAT_159 (continuous surface cap model, or CSCM). CSCM is normally used in the simulation of concrete components subjected to impact and blast loads [13, 19]. The uniaxial compressive strength of concrete is 30, 40 and 50 MPa and the corresponding material parameters are automatically generated by the CSCM in LS-DYNA. The CSCM considers the cap formula to describe the compaction of concrete materials. When the calculated stress is outside the yield surface, the plasticity algorithm is used to restore the stress state to the yield surface. Hardening and strain rate effects are also incorporated into the CSCM material model. Concrete materials are pressure-related materials. According to elastic-plastic theory, the general form of the yield failure equation is:

$$f(J_1, J_2, J_3) = 0 \tag{1}$$

where J_1 is the first stress tensor invariant; J_2 is the second stress tensor invariant; J_3 is the third stress tensor invariant.

The yield function of the CSCM is expressed by:

$$f(J_1, J'_2, \beta, \kappa) = J'_2 - \Re^2(\beta) F_f^2(J_1) F_C(J_1, \kappa) \tag{2}$$

where $F_f^2(J_1)$ represents the shear failure surface; $F_C(J_1, \kappa)$ is the hardening cap; κ is the hardening parameter; J'_2 is the second deviatoric stress invariant; $\Re(\beta)$ is the reduction factor.

The reinforcements are simulated using *MAT_PLASTIC_KINEMATIC, i.e., a bilinear elastic-plastic model [20]. This model is an elastic-plastic, strain-hardening and strain-rate hardening model. This material model measures the initial yield stress through two factors: the strain factor and the strain rate factor. The yield stress can be written as follows.

$$\sigma_y = [1 + (\frac{\dot{\varepsilon}}{C})^{(\frac{1}{p})}](\sigma_0 + \beta E_p \varepsilon_{eff}^p) \tag{5}$$

where σ_0 is the initial yield stress of reinforcement under static load; β is the strain hardening parameter; ε_{eff}^p is the effective plastic strain; $\dot{\varepsilon}$ is the strain rate; p and C are strain rate parameters; E_p is the plastic hardening modulus of reinforcement, which is represented by the elastic modulus E and the tangent elastic modulus E_{tan}, as shown in Equation (6):

$$E_p = \frac{E_{tan} E}{E - E_{tan}} \tag{6}$$

According to the failure strain criterion, when the strain of the longitudinal bars and stirrups reaches a certain strain threshold (ε_f), the longitudinal bars and stirrups are failure. The failure strain of longitudinal reinforcement and stirrup is set as 0.25 and 0.20, respectively [1]. The rigid material (*MAT_RIGID) is selected for the rockfalls because the damage of rockfalls is not the focus [1]. To simplify the calculation, the rockfall is simulated by the sphere which is widely used in previous studies [1]. According to extensive on-site investigation in the previous studies, granites are most frequently found in the rockfall accidents [26, 27]. Hence, the rockfall was assumed to be granite with a gravity of 2.5-3.0 g/cm3 [1]. Moreover, the previous studies found that the rockfall only appears slighter damage compared with concrete pier [26, 27]. Therefore, the rockfall is regarded as a rigid material and the material parameter is listed in Table 2.

Table 2. Material parameters.

Preprints (www.preprints.org) | NOT PEER-REVIEWED | Posted: 20 September 2022 doi:10.20944/preprints202209.0274.v2

Material type	Keywork in LS-DYNA	Parameter	Value
Transverse reinforcement	*MAT_PLASTIC_KINEMATIC	Elastic modulus (GPa)	210
		Density (g/cm^3)	7.85
		Poisson's ratio	0.3
		Failure strain	0.25
		Yield strain (MPa)	300
Longitudinal reinforcement	*MAT_PLASTIC_KINEMATIC	Elastic modulus (GPa)	210
		Density (g/cm^3)	7.85
		Poisson's ratio	0.3
		Failure strain	0.2
		Yield strain (MPa)	400
Rockfall	*MAT_RIGID	Elastic modulus (GPa)	26.0
		Density (g/cm^3)	2.6
		Poisson's ratio	0.22

2.3 Verification

2.3.1 Verification against two experiments

This material model and contact algorithm of the rock-HTWBP model are verified based on the drop weight test of reinforced concrete beam performed by Fujikake et al. [21]. As shown in Figure 5, the test drops a weight of 400 kg from four different heights on the middle of the span of concrete reinforced beams. The lower part of the drop hammer has a hemispherical tip with a radius of 90 mm. In the test, the concrete reinforced beam has a rectangular cross-section of 150×250 mm, the length of the beam is 1700 mm, and the uniaxial compressive strength of the concrete is 42 MPa. The diameters of the longitudinal reinforcement of the three tests are 16, 22 and 22 mm with yield strengths of 397, 426 and 418 MPa, respectively. The diameter of the transverse reinforcement is 10 mm with a spacing of 75 mm, and the yield strength is 295 MPa. The reinforcement is shown in Figure 6. One of the reinforcement conditions is selected for verification, that is, the longitudinal reinforcement diameter is 16 mm, the longitudinal reinforcement ratio is 1.26%, and the impact height of the drop hammer is 0.15m, 0.3m, 0.6m, 1.2m. Figure 7 shows the FE model established based on the above tests. The material models and contact algorithm are consistent with Sections 2.1 and 2.2.

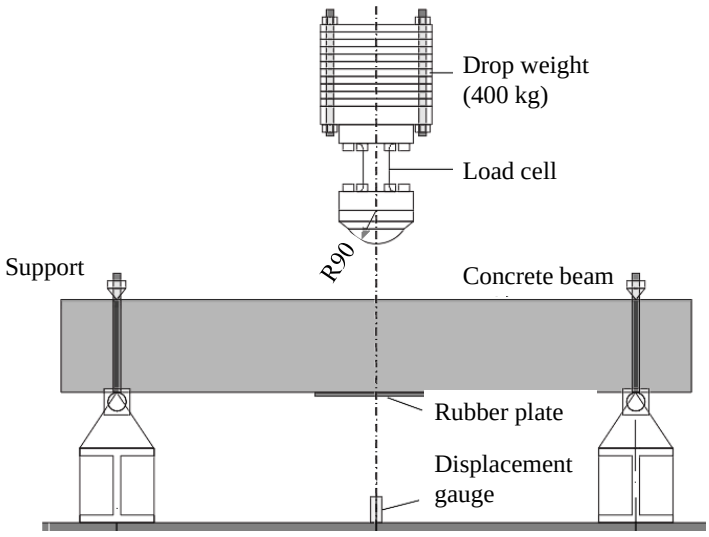

Figure 5. The drop weight test [21].

 doi:10.20944/preprints202209.0274.v2

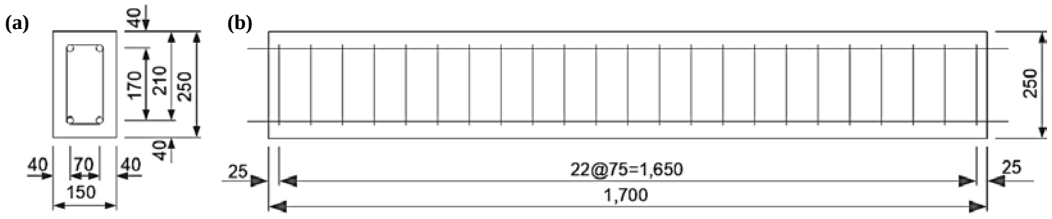

Figure 6. The reinforcement [21]: (a) Cross-sectional view; (b) Front view.

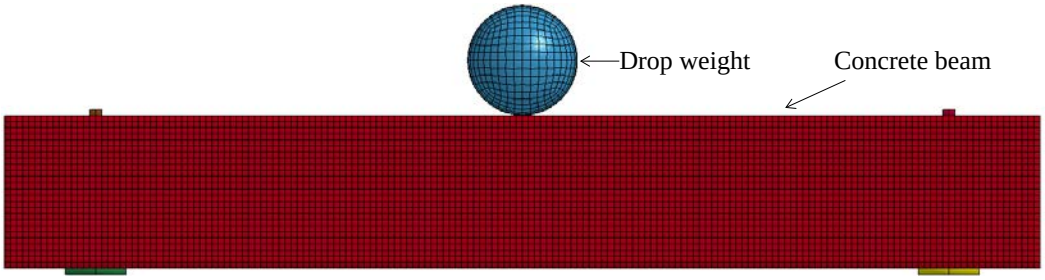

Figure 7. FE model of the drop weight test.

Figure 8 compares the damage between the experiment and FE analysis at different impact heights. As shown in the figure, at different impact heights, the concrete beam in the experiment and FE analysis exhibits overall flexural failure, and bending cracks appear on the lower side. Moreover, when the height of the drop weight is 1.2 m, it is observed that serious local damage occurs at all loading positions. The damage mode obtained in the FE model is in good agreement with the damage phenomenon observed in the impact experiment, which indicates that the FE model can accurately simulate the damage of the concrete beam under the impact load.

Figure 9 compares the time history curves of mid-span displacement and impact force when the impact height is 1.2 m. As shown in Figure 9, the variation trend and peak value of the mid-span displacement time history curve between the experiment and FE analysis are very close, and the difference of peak value is only 0.3%. For the impact force time history curves, the two curves have some differences, which may be caused by the test conditions or the discreteness of the FE simulation, but the peak values of the two curves are almost equal, and the difference is only 0.8%. In the field of concrete impact, the peak impact force is usually taken as the focus of research, so the difference in the curve shape can be ignored as a secondary factor. In addition, the peak impact force and mid-span displacement of the experiment and FE analysis under different impact heights are compared in Table 3, and the maximum error is 2.8%. The above analysis shows that the finite element model has a high reliability in predicting the dynamic response of reinforced concrete beams under impact load, and the CSCM concrete material model can better simulate and analyze the damage and dynamic response of reinforced concrete beams under impact.

 doi:10.20944/preprints202209.0274.v2

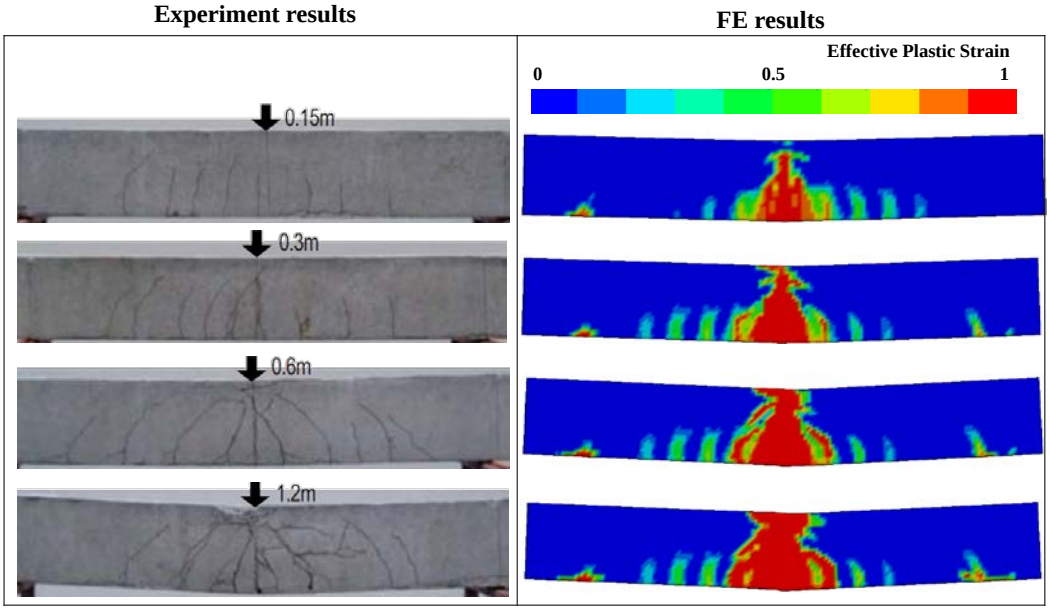

Figure 8. Comparison of damage between the experiment and FE analysis.

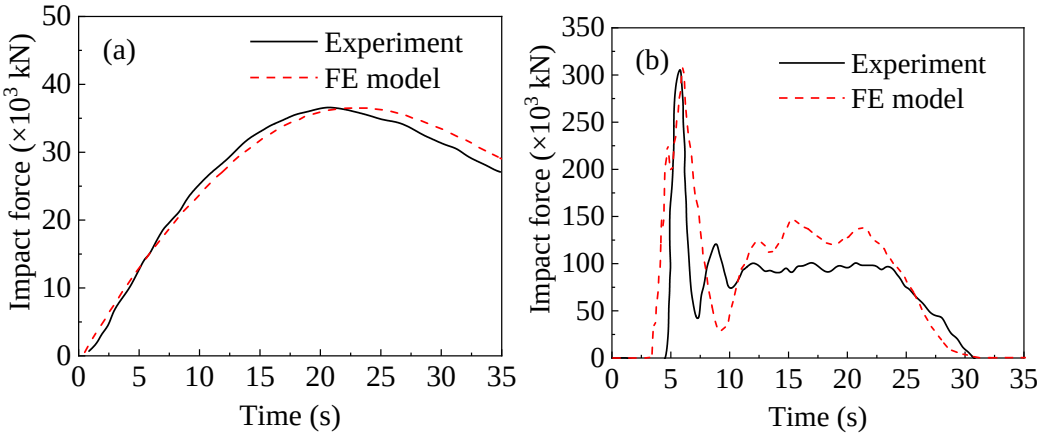

Figure 9. Comparison between experiment [21] and FE analysis: (a) Mid-span displacement; (b) Impact force.

Table 3. Comparison of peak impact force and mid-span displacement

Impact height	Peak impact force (kN)			Mid-span displacement (mm)		
	Experiment [21]	FE analysis	Difference	Experiment [21]	FE analysis	Difference
0.15 m	124.3	125.8	1.2%	6.1	6.2	1.6%
0.30 m	182.7	180.9	1.0%	10.9	10.6	2.8%
0.60 m	243.8	250.7	2.8%	20	20.2	1.0%
1.20 m	308.4	310.9	0.8%	36.6	36.5	0.3%

Preprints (www.preprints.org) | NOT PEER-REVIEWED | Posted: 20 September 2022 doi:10.20944/preprints202209.0274.v2

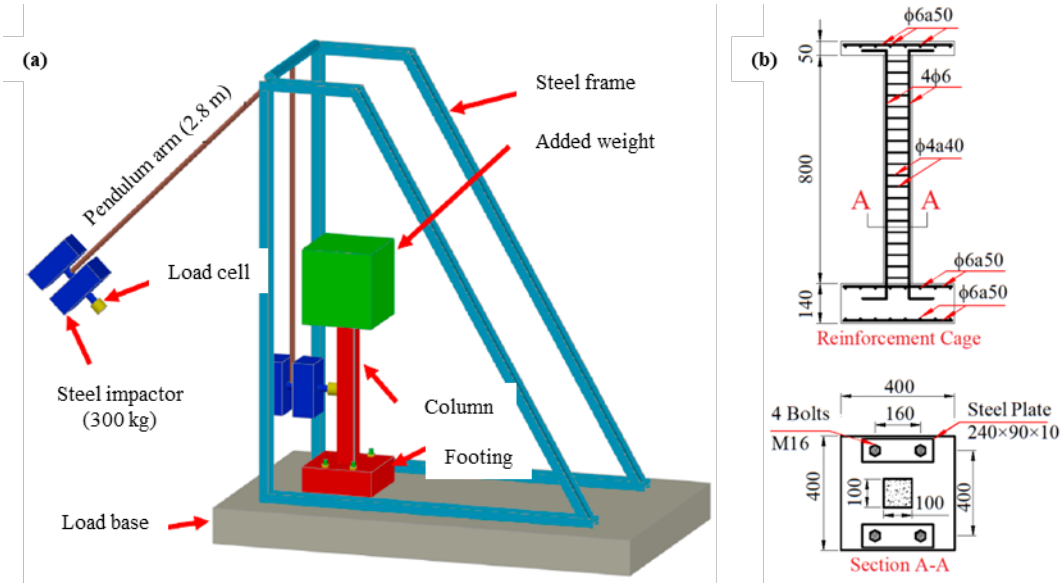

Figure 10. 3D view of the experiment setup and reinforcement of the column [28].

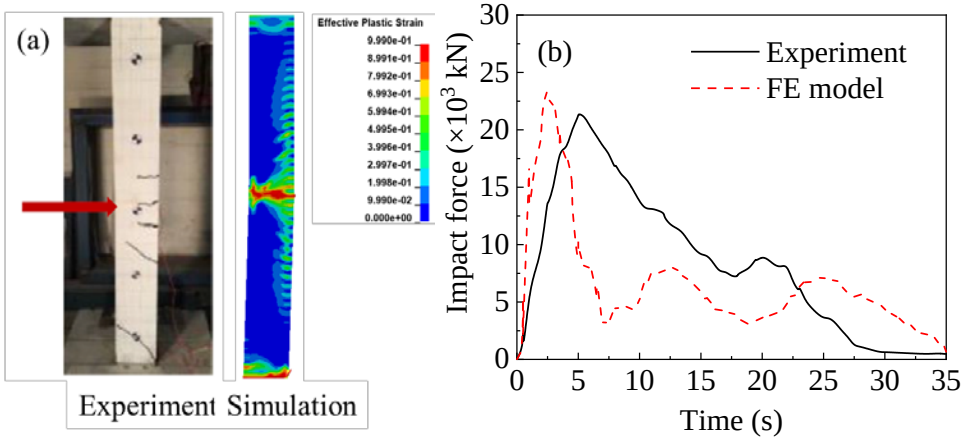

Figure 11. Comparison between experiment in [28] and FE analysis: (a) Damage pattern; (b) Impact force.

Considering the end condition for the beams in [21] and the HTWBP are different, a column-pendulum experiment conducted by Zhang et al. is selected here for further verification [28]. In the experiment, the column has a 400×400 mm square cross-section and a height of 800 mm. An added weight of 288 kg is exerted on the top of the column to make the end condition similar to a real bridge. The pendulum is made of steel and weighs 300 kg, impacting the column at a speed of 0.64 m/s. More detailed information can be found in Ref. [28]. Figure 10 presents the 3D view of the experiment setup and reinforcement of the column.

A 1:1 FE model is established according to the details of the experiment. Figure 11 shows the comparison between the experiment in [28] and FE analysis. As shown in Figure 11(a), the damage pattern of the experiment and simulation is similar. Specifically, the simulation well captures the flexural and shear cracks. As shown in Figure 11(b), the impact force undergoes a similar up-down process in both the experiment and simulation. Although the two curve shapes show a moderate difference, the peak impact forces are close. The error of the simulation is only 9.3%, which is acceptable when considering an engineering problem. Hence, the verification process further proves that the FE models established in this research are reliable.

2.3.2 Mesh independence verification

Preprints (www.preprints.org) | NOT PEER-REVIEWED | Posted: 20 September 2022 doi:10.20944/preprints202209.0274.v2

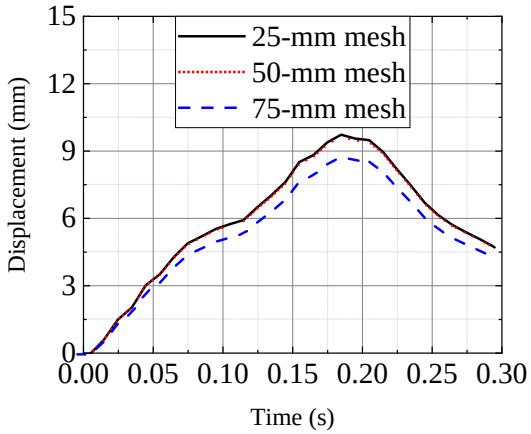

Figure 12. Mesh independence verification.

To verify the rationality of the mesh size for the impacted pier, a grid independence verification is conducted. Three mesh sizes, i.e., 25, 50 and 75 mm, are adopted to mesh the impacted pier. Figure 12 compares the mid-span displacement of the impacted under three mesh sizes. As shown in Figure 12, the results obtained by the 25-mm mesh and 50-mm mesh are consistent with only 1% difference observed. However, the displacement calculated by the 75-mm mesh shows large difference with 25-mm and 50-mm meshes. Hence, it is believed the 75-mm mesh is too large to simulate the impact behavior of the HTWBP. To balance the accuracy and computational efficiency, adopting the 50-mm mesh for the impacted pier is reasonable.

3 Rockfall impact resistance of

Based on the rockfall-HTWBP model established in Section 2, the impact resistance of HTWBP under different impact parameters is analyzed in this section. The involved parameters are: impact height h, impact velocity v of rockfall, rockfall diameter d, and strength grade s of concrete. Considering the rockfall normally impacts the middle and below parts of the pier, for the bridge pier with a total height of 80 m in this paper, the impact height ranges is 10-40 m. The impact velocity v is 30, 20 and 10 m/s, respectively. The diameter d of rockfall is 1.5 to 4.0 m, and the concrete strength (uniaxial compressive strength) s of is 30, 40 and 50 MPa respectively. The rockfall size is determined according to two previous research [1, 2]. In the study of Xie et al., 2020, three rock diameters, i.e., 1.2 m, 1.5 m and 1.8 m, are considered [1]. In another reference [2], the rockfall diameters range from 0.4 m to 4 m. However, the rockfall with a diameter of lower than 1.0 m is considered to have limited influence on the pier. Table 4 summarizes the cases used in this section.

Table 4. Investigated cases.

Case	h (m)	v (m/s)	d (m)	s (MPa)
C1(Reference case)	40	20	1.5	30
C2	10	20	1.5	30
C3	20	20	1.5	30
C4	30	20	1.5	30
C5	40	10	1.5	30
C6	40	30	1.5	30
C7	40	20	2	30
C8	40	20	2.5	30
C9	40	20	3.0	30

 doi:10.20944/preprints202209.0274.v2

C10	40	20	3.5	30
C11	40	20	4.0	30
C12	40	20	1.5	40
C13	40	20	1.5	50

3.1 Impact force characteristic

The time history curves of impact force in different cases are shown in Figure 13. As shown in Figure 13, the impact force of rockfall has a significant impulse characteristic, and the duration of the impulse load is approximately 0.01s. In addition, the impact process only lasts less than 0.05 s, indicating that the rockfall impact on bridge pier is a transient dynamic problem. At t=0 s, the rockfall starts to contact the bridge pier, and the impact force increases rapidly and reaches the peak value in a very short time (0.005 s). After the rockfall contacts the pier, the instantaneous impact effect increases the local velocity of the pier and decreases the velocity of the rockfall. Then the rockfall separates with the pier, so the impact force decreases rapidly after reaching the peak value. Because the bridge pier has a certain elasticity, the concrete is in an elastic vibration state after being impacted by the rockfall, so the time history curve of subsequent impact force still fluctuates.

As shown in Figure 13(a), when the impact height is 10, 20, 30 and 40 m, the peak impact force is 34.8×10³ kN, 33.4×10³ kN, 31.3×10³ kN and 29.4×10³ kN, respectively. When the impact height increases from 10 m to 40 m, the peak impact force decreases by 15.5%. The possible reason for this phenomenon is that when the impact position is closer to the pile cap, the pier is constrained more strongly and the corresponding peak impact force is larger. As shown in Figure 11(b), (c) and (d), the peak impact force increases with the increase of impact velocity, rockfall diameter and concrete strength. When the impact velocity increases from 10 m/s to 30 m/s, the peak impact force increases by 170.1%. When the rockfall diameter increases from 1.5 m to 4.0 m, the peak impact force increases by 100.0%. This is because the larger the velocity and diameter of the rockfall, the larger the corresponding kinetic energy, leading to the increase of the impact force. When the concrete strength grade increases from 30 MPa to 50 MPa, the peak impact force only increases by approximately 5%. This indicates that the impact force mainly depends on the stiffness of the rockfall, while the stiffness of the bridge pier plays a secondary role, which is consistent with the research results of [1].

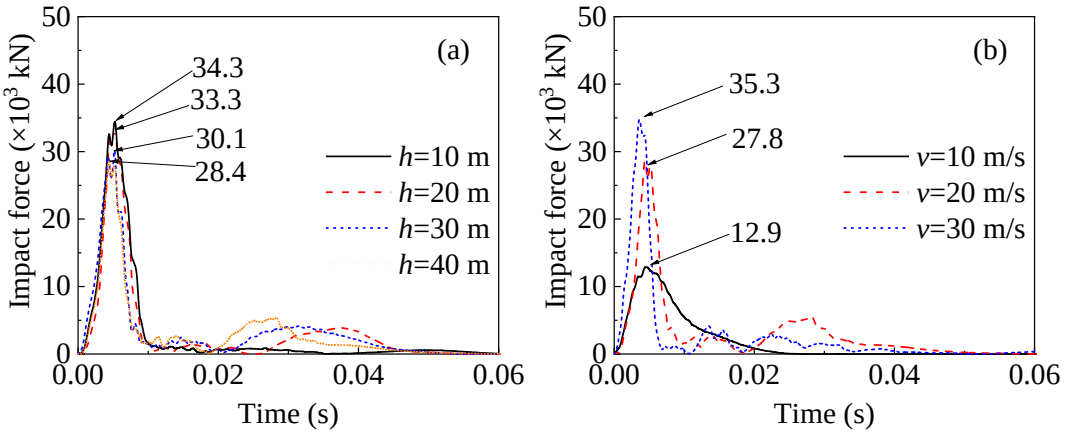

Preprints (www.preprints.org) | NOT PEER-REVIEWED | Posted: 20 September 2022 doi:10.20944/preprints202209.0274.v2

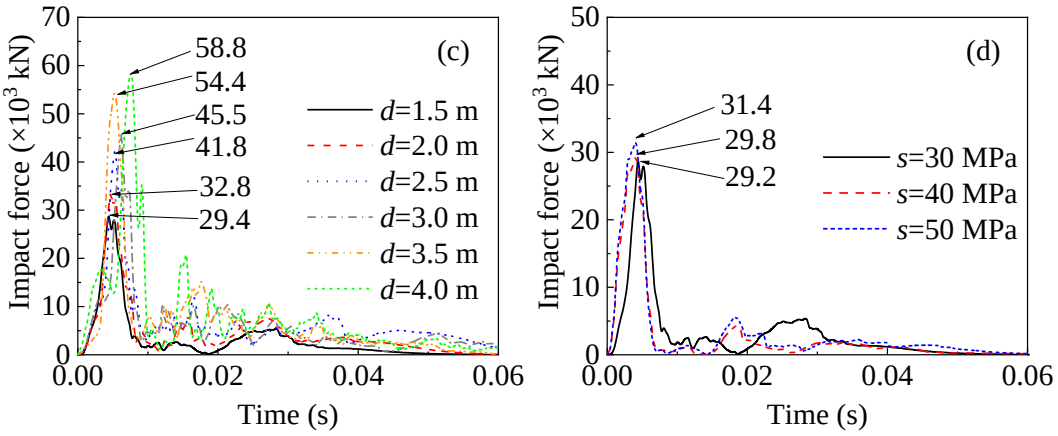

Figure 13. Impact force of rockfall-HTWBP impact.

3.2 Damage characteristic

Element killing algorithm (*MAT_ADD_EROSION) in LS-DYNA is used to simulate the damage of bridge piers impacted by rockfalls [22]. To make the FE simulation result close to the actual impact result, the maximum principal strain of 0.1 is set as the condition of mesh killing. Figure 14 shows the damage process of impacted surface and side surface of the pier when h=40 m (Case C1). Figure 15 shows the damage process of the mid-height cross-section.

As shown in Figure 14(a), when the HTWBP is impacted by rockfall, an elliptical damage centered on the rockfall appears on the impacted surface of the pier, and the damage degree gradually deepens and spreads along the pier vertically and toward the pier edge. When t=0.006 s, that is, after the impact force reaches the peak, the damage degree is relatively light. When t= 0.008 s, the damage degree gradually deepens, and the damage area spreads both vertically and to the edge of the bridge pier. There are conical and strip damage areas at the edge of the pier and the vertical center line of the pier respectively, which may be caused by the weak transverse flexural bearing capacity of the impacted surface of the hollow pier. As the impact process continues, the conical and strip damage areas further extend, and the degree of damage gradually aggravates. At the same time, the damage area of the impacted surface gradually develops into the final elliptic damage with the conical and strip damage areas as the symmetry axis. In addition, the time of impact force is about t=0.005 s, while the damage process of bridge pier mainly occurs from t=0.006 s to t=0.300 s. This phenomenon shows that the bridge pier has a lag effect on the dissipation of the impact energy, so it takes a certain time for the kinetic energy to be converted into internal energy after the rockfall impact.

As shown in Figure 14(b), when t= 0.006s, no evident damage is observed on the side surface of the bridge pier, because the damage caused by the impact force has not been transmitted to the side surface of the bridge pier. When t= 0.008s, there is a triangular compression damage area near the impacted surface on the side surface of the pier, which is consistent with the conical damage area at the pier edge at t=0.008s in Figure 14(a). The triangular damage area continues to expand vertically to the back of the pier, and the damage degree continues to intensify, and finally develops into a radial damage area across the side surface of the pier. At the same time, one side of the damage area close to the impact point has serious damage, whereas the other side only shows slight tensile damage.

Preprints (www.preprints.org) | NOT PEER-REVIEWED | Posted: 20 September 2022 doi:10.20944/preprints202209.0274.v2

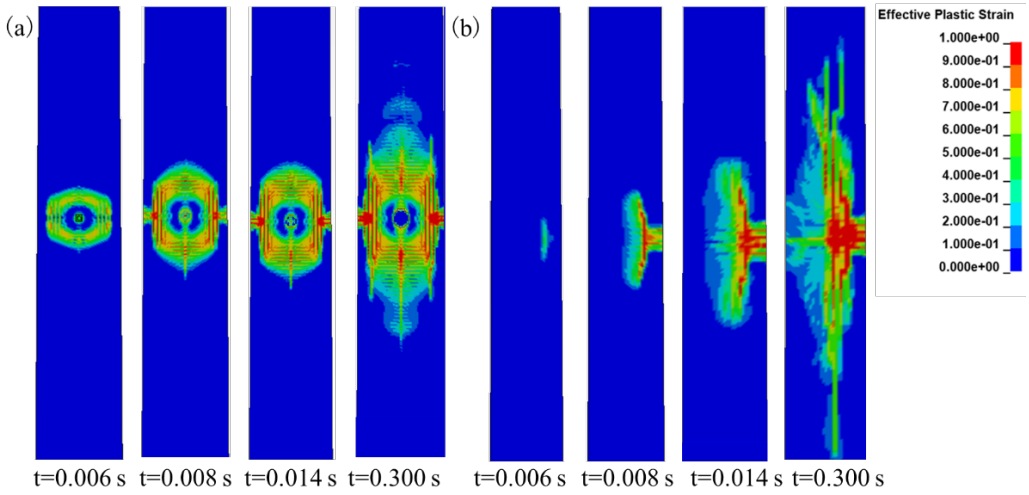

Figure 14. Damage process of the pier (*h*=40 m): (a) Impacted surface; (b) Side surface.

As shown in Figure 15, when t=0.006 s, the damage begins to appear on the impacted surface of bridge pier, and because the inner side of the impacted surface of bridge pier is in a tensile state, the damage degree of the inner side is greater than that of the outer side. When t= 0.008 s, the damage extends to the whole impacted surface, especially at the corner, and the concrete falls off because of the impact. Two symmetrical slender shear damage areas at the corner of the back side of the pier are observed. When t=0.014 s, the shear damage area on the back side of the bridge pier extends through the cross-section, and the damage degree of the impacted surface further aggravates. When t= 0.300 s, the concrete in the impact area of the impacted surface is deleted. In addition, similar to the impacted surface and side surface of the pier, the damage process of the cross section mainly occurs after the impact force reaches the peak value, namely, after t=0.006 s. In general, the cross-sectional damage modes of the HTWBP subjected to rockfall impact is compression failure in the impact area and shear failure at the corner.

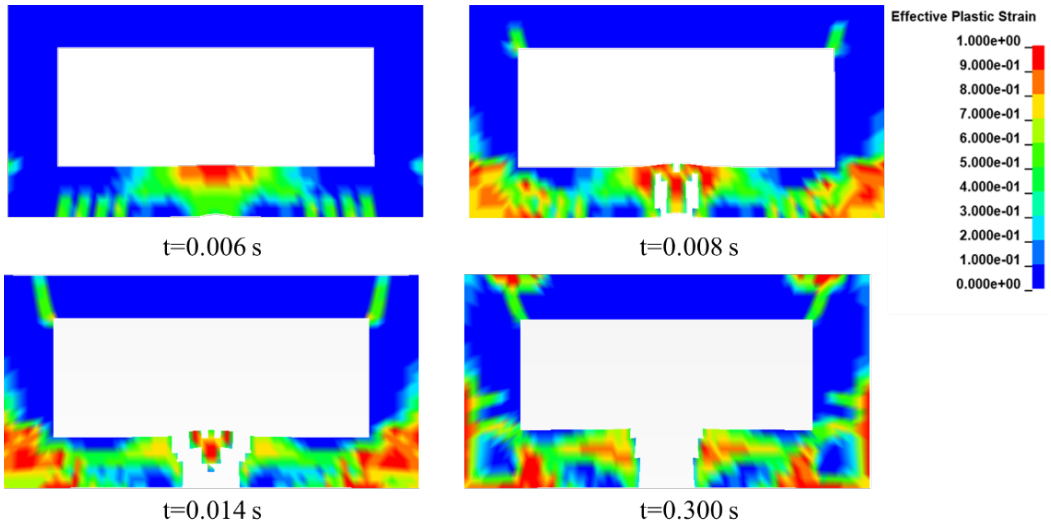

Figure 15. Damage process of the cross-section (*h*=40 m).

3.3 Deformation characteristic

Figure 16 shows the displacement time history curves of each cross-section of the pier when the impact height *h*=40 m, where 0 m is the pier bottom and 80 m is the pier top. After the impact, the displacement of the impacted cross-section (40 m) first increases, and then the stress wave propagates up and down from the impact position at the

Preprints (www.preprints.org) | NOT PEER-REVIEWED | Posted: 20 September 2022 doi:10.20944/preprints202209.0274.v2

same speed, so the displacement of 30 m and 50 m cross-sections almost increased at the same time. It can also be found that the initial growth rate of displacement of 30 m and 50 m cross-sections is basically the same. The same phenomenon is also observed in 20 m and 60 m cross-sections and 10 m and 70 m cross-sections. The maximum displacement of the nine sections is 9.77 mm, which appears at the impacted cross-section. The maximum displacement appears at 40 m height because the superstructure gravity exerts a strong constraint on the pier top. In other words, when the pier top tries to move, it has to resist a huge inertial force of the superstructure.

The displacement of the top and bottom of the pier is significantly lower than that of other cross-sections due to constraints. The time when the maximum displacement occurs of the cross-sections below the impact position is earlier than the cross-sections upper the impact position, because the upper part of the pier has greater flexibility and is more prone to deformation.

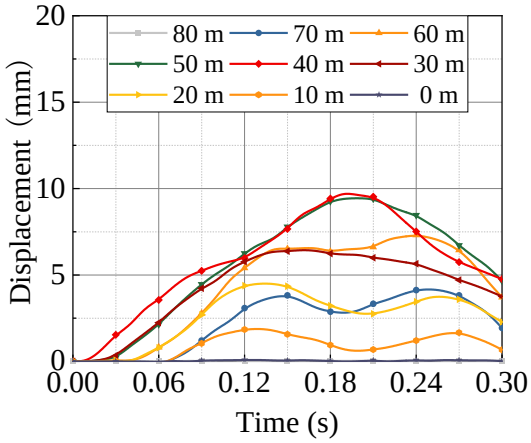

Figure 16. Displacement time history curves (Case C1).

Figure 17 shows the maximum displacement of each cross-section of the pier in different cases. As shown in Figure 17, when the impact parameters change, the maximum displacement of each section of the pier appears on the back side. The displacement of pier top and bottom is zero due to the constraint of superstructure and cap. Under different cases, the maximum displacement occurs in 40 m to 60 m of the pier height. This is because the HTWBP studied in this paper has a smaller cross-section at the top and a larger cross-section at the bottom. The lower part of the pier has a larger stiffness and a stronger ability to resist deformation.

As shown in Figure 17, the maximum displacement increases with impact height, impact velocity and rockfall diameter. The maximum displacement of bridge pier decreases with the increase of concrete strength. As shown in Figure 17(a), the maximum displacement is 4.8, 7.6, 9.5 and 9.8 mm when the impact height is 10, 20, 30 and 40 m, respectively. When the impact height rises from 10 m to 40 m, the maximum displacement increases by 104.2%. This is due to the fact that the closer the impact position is to the pier top, the weaker the cross-section and therefore the greater the displacement. As shown in Figure 17(b), when the initial impact velocity of rockfall is 30, 20 and 10 m/s, the maximum displacement is 12.37 mm, 9.77 mm and 6.03 mm, respectively. When the initial impact velocity of rockfall increases from 10 to 30 m/s, the maximum displacements increase by 100.3%. As shown in Figure 17(c), when the diameter of rockfall is 1.5, 2.0 m, 2.5 m, 3.0 m, 3.5 m and 4.0 m, the maximum displacements are 9.77, 14.7, 27.58, 35.5, 44.7 and 56.1 mm, respectively. When the diameter of rockfall increases from 1.5 m to 4.0 m, the maximum displacements of bridge piers increase by 474.2%. The rockfall diameter has a significant influence on the displacement of bridge pier. When the rockfall diameter increases, the deformation of bridge pier increases. As shown in Figure 17(d), when the bridge pier concrete strength grades are 30, 40 and 50 MPa, the maxi-

Preprints (www.preprints.org) | NOT PEER-REVIEWED | Posted: 20 September 2022 doi:10.20944/preprints202209.0274.v2

mum displacements are 7.6, 4.2 and 3.9 mm, respectively. When the concrete strength grade increases from 30 to 40 MPa, the maximum displacement decreases by 44.7%. When the concrete strength grade increases from 40 to 50 MPa, the maximum displacement decreases by 7.1%. This indicates that the improvement of concrete strength grade can effectively increase the impact resistance because of the improvement in pier stiffness.

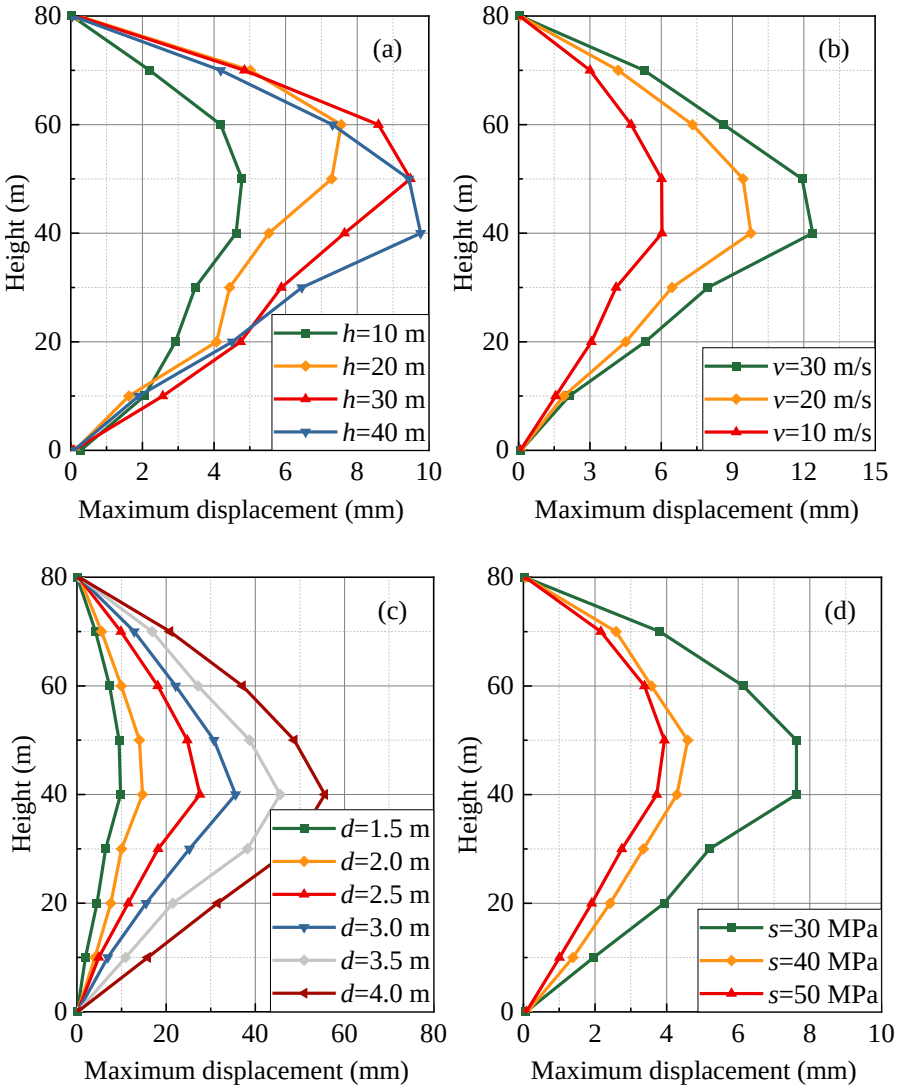

Figure 17. Maximum displacement of the HTWBP.

4 Damage assessment criteria based on response surface model

4.1 Definition of damage index

Based on the damage function of the CSCM, which considers the softening and modulus reduction, the brittle damage parameter $d(\tau_t)$ and ductile damage parameter $d(\tau_c)$ can be calculated as follows:

$$d(\tau_t) = \frac{0.999}{D}\left[\frac{1+D}{1+De^{-C(\tau_t-\tau_{0t})}}\right] \tag{3}$$

$$d(\tau_c) = \frac{d_0}{B}\left[\frac{1+B}{1+Be^{-A(\tau_c-\tau_{0c})}}-1\right] \tag{4}$$

Preprints (www.preprints.org) | NOT PEER-REVIEWED | Posted: 20 September 2022 doi:10.20944/preprints202209.0274.v2

where A, B, C and D are softening parameters; d_0 is the maximum damage level in simulation; τ_t and τ_c are brittle and ductile damage level respectively; τ_{0t} and τ_{0c} are brittle and ductile damage thresholds respectively.

Therefore, based on the element damage factor d_e calculated by the CSCM, the volume damage index d_v of the HTWBP volume is defined as follows:

$$d_v = \frac{1}{n}\sum_{1}^{n} d_e \tag{7}$$

$$d_e = d(\tau_t) + d(\tau_c) \tag{8}$$

where n is the total element number of the impacted pier.

Because the damage of bridge pier is generally local and the volume of damaged concrete is small, to facilitate expression and comparison, the volume damage factor d_v is normalized, and the corresponding damage index D can be expressed as follows.

$$D = \frac{d_v}{d_{max}} \tag{9}$$

where d_{max} is the maximum volume damage factor for all cases in this paper.

4.2 Establishment of the response surface model

To improve computational efficiency, response surface method is widely used as an alternative model in parameter sensitivity analysis and design optimization [23]. The response surface method assumes that the response of the structure can be approximated by:

$$\tilde{y}(x) = \sum_{i=1}^{n} a_i \varphi_i(x) \tag{10}$$

where $\tilde{y}(x)$ is the structure response; $\varphi_i(x)$ is the basis function; n is the number of basis functions; a_i is the response surface function coefficients.

According to the least square method, the response surface function coefficient is determined as:

$$a = (\Phi^T \Phi)^{-1}(\Phi^T y) \tag{11}$$

where a is the response surface function coefficient matrix and $a = [a_0, a_1, \cdots, a_n]$; Φ is the matrix formed by the sample points and is expressed as follows:

$$\Phi = \begin{bmatrix} \varphi_1(x^{(1)}) & \cdots & \varphi_n(x^{(1)}) \\ \vdots & \vdots & \vdots \\ \varphi_1(x^{(i)}) & \cdots & \varphi_n(x^{(i)}) \\ \vdots & \vdots & \vdots \\ \varphi_1(x^{(m)}) & \cdots & \varphi_n(x^{(m)}) \end{bmatrix} \tag{12}$$

By solving the matrix equation of response surface random variables, the response surface function coefficients can be solved, and the response surface function $\tilde{y}(x)$ can be obtained.

The response surface method incorporates many factor design methods, including orthogonal design method, Central Composite Design method, Box-Behnken Design method. To study the rockfall impact resistance of HTWBP, if the complete factorial design is adopted for the four parameters of three levels, then a total of 3^4=81 FE simulations need to be involved. Hence, Box-Behnken design is adopted to reduce the number of FE simulations and improve the computational efficiency of sensitivity analysis. Table

Preprints (www.preprints.org) | NOT PEER-REVIEWED | Posted: 20 September 2022 doi:10.20944/preprints202209.0274.v2

5 shows the factors and levels of Box-Behnken design in this section. According to the Box-Behnken design in Table 5, corresponding cases and damage results are listed in Table 6. According to the data in Table 6, the response surface model can be expressed as Equation (13).

Table 5. Factors and levels of Box-Behnken design.

Factor	Level		
	-1	0	1
h (m)	20	40	60
v (m/s)	10	20	30
d (m)	1.5	2.0	2.5
s (MPa)	30	40	50

Table 6. Box-Behnken design cases and damage results.

Std	Run	h (m)	v (m/s)	d (m)	s (MPa)	d_v (×10^{-3})	D
1	24	20	10	2	40	0.89	0.156
2	28	60	10	2	40	0.67	0.117
3	17	20	30	2	40	1.49	0.260
4	9	60	30	2	40	1.61	0.281
5	16	40	20	1.5	30	1.12	0.196
6	7	40	20	2.5	30	1.32	0.231
7	12	40	20	1.5	50	0.89	0.156
8	23	40	20	2.5	50	1.63	0.285
9	4	20	20	2	30	1.20	0.210
10	22	60	20	2	30	1.14	0.199
11	18	20	20	2	50	1.13	0.198
12	5	60	20	2	50	0.93	0.162
13	21	40	10	1.5	40	0.78	0.136
14	8	40	30	1.5	40	1.16	0.203
15	29	40	10	2.5	40	1.16	0.203
16	15	40	30	2.5	40	1.95	0.341
17	6	20	20	1.5	40	1.00	0.175
18	2	60	20	1.5	40	1.00	0.175
19	27	20	20	2.5	40	1.62	0.283
20	14	60	20	2.5	40	1.39	0.243
21	1	40	10	2	30	0.93	0.163
22	11	40	30	2	30	1.48	0.259
23	10	40	10	2	50	1.08	0.189
24	26	40	30	2	50	1.51	0.264
25	3	40	20	2	40	1.02	0.178
26	25	40	20	2	40	0.99	0.173
27	20	40	20	2	40	1.11	0.194
28	19	40	20	2	40	1.01	0.177
29	13	40	20	2	40	0.94	0.164

$$d_v = 10^{-6} \times \begin{pmatrix} 7926 + -8.5625h - 222.45v - 3687.834d \\ -95.49167s + 0.845hv - 5.75hd - 0.18125hs \\ +40.9vd - 0.6vs + 26.8ds + 0.09927084h^2 \\ +4.808334v^2 + 636.8334d^2 + 0.762083s^2 \end{pmatrix} \quad (13)$$

Preprints (www.preprints.org) | NOT PEER-REVIEWED | Posted: 20 September 2022 doi:10.20944/preprints202209.0274.v2

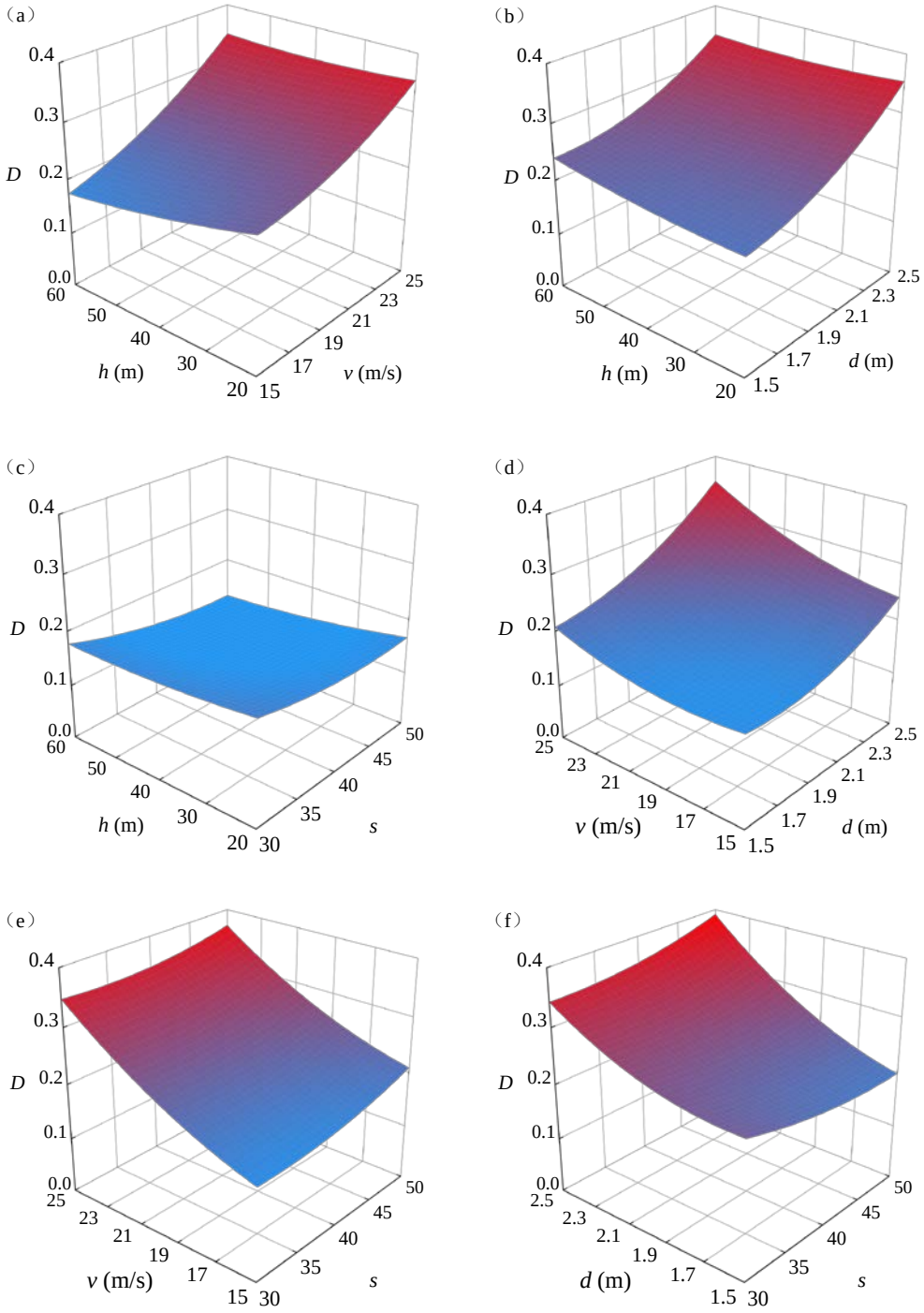

Figure 18. Damage response surfaces with different parameters

Figure 18 shows the damage response surfaces with different parameters obtained from the response surface model expressed in Equation (13). In each subfigure, the influence of two parameters is presented and other parameters are fixed at level 0 as listed in Table 5. As shown in Figure 18, different parameters have dissimilar effects on the damage indices when they are impacted by rockfalls. As shown in Figure 18(a) and (b), with the increase of the initial impact velocity and rockfall diameter, the damage factor increases significantly, and the influence of the initial impact velocity and rockfall diameter is greater than the impact height. As shown in Figure 18(c), with the increase of the impact height and concrete strength, the damage factor of the HTWBP slightly changes. As shown in Figure 18(e) and (f), the damage factor increases significantly with the in-

Preprints (www.preprints.org) | NOT PEER-REVIEWED | Posted: 20 September 2022 doi:10.20944/preprints202209.0274.v2

crease of the initial impact velocity and diameter of rockfall, which is more significant than that of the concrete strength. It can be seen from the six response surfaces in Figure 18 that the initial impact velocity and diameter of the rockfall are the most significant parameters affecting the damage indices, followed by the impact height and concrete strength, i.e., $v \approx d > h \approx s$.

Six FE models are supplemented to further verify the accuracy of the established response surface model, as listed in Table 7. The damage index calculated by using the FE model and predicated by the RSM is also compared in Table 7 and Figure 19. The determination coefficient R^2 and relative error (RE) are used to evaluate the accuracy of the model. As listed in Table 7 and shown in Figure 19, the maximum difference between the FE model and predicated by the RSM is only 4.8%. The determination coefficient R^2 value is 0.9610, which is close to 1.0, and the average RE is only 4.5%. Therefore, the response surface model established expressed in Equation (13) shows high competence in predicting the damage of HTWBP after rockfall impact.

Table 7. Supplemented cases for verification of the response surface model.

Run	h (m)	v (m/s)	d (m)	s (MPa)	D		Difference
					FE results	RSM results	
30	40	20	1.5	50	0.16	0.15	4.8%
31	40	20	1.5	40	0.16	0.16	1.2%
32	40	20	2	30	0.19	0.19	1.6%
33	40	15	1.5	30	0.19	0.18	4.7%
34	40	25	2.5	30	0.35	0.34	2.7%
35	60	20	2.5	30	0.24	0.24	3.2%

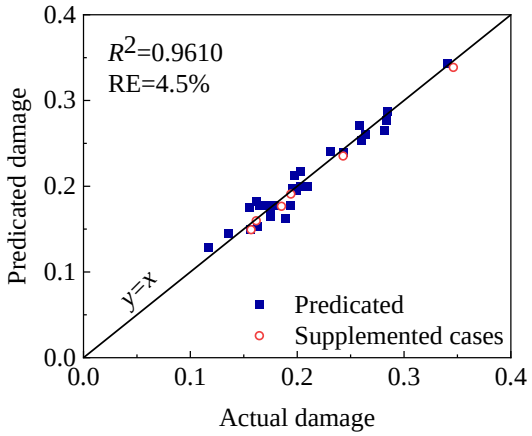

Figure 19. Verification of the response surface model.

4.3 Damage assessment method

Considering the impact velocity and rockfall diameter are the most influential parameters on the damage, the two parameters are used as the controlling parameters of the damage assessment method. In this section, the central composite design is used to expand the parameter range of controlling parameters and establish the damage assessment curve. The central composite design is the most commonly used second-order design method in response surface analysis. On the basis of two-level factor design, a small number of center points and star points are added to make each factor have five levels for response surface analysis.

The impact height is set as 40 m, and the strength grade is set as 30 MPa. Table 8 shows the factors and levels of the central composite design in this section. According to the central composite design in Table 8, corresponding cases and damage results are

Preprints (www.preprints.org) | NOT PEER-REVIEWED | Posted: 20 September 2022 doi:10.20944/preprints202209.0274.v2

listed in Table 9. According to the damage results in Table 9, the response surface function can be expressed as Equation (14). Figure 20 shows the response surface of the damage index under different impact velocity and rockfall diameter. As shown in Figure 20, the damage index significantly increases with the increases in impact velocity and rockfall diameter. This phenomenon is consistent with the aforementioned results.

Table 8. Factors and levels of the central composite design.

Factor	Level				
v (m/s)	10	20	30	40	50
d (m)	1.0	1.375	1.75	2.125	2.5

Table 9. the central composite design cases and damage results

Std	Run	V (m/s)	D (m)	d_v (×10^{-3})	D
1	2	10	1	0.0476	0.01
2	8	50	1	2.61	0.46
3	9	10	2.5	1.24	0.22
4	6	50	2.5	5.72	1.00
5	3	20	1.75	2.18	0.38
6	5	40	1.75	3.84	0.67
7	1	30	1.375	2.43	0.42
8	7	30	2.125	3.49	0.61
9	4	30	1.75	2.81	0.49
10	4	30	1.75	3.14	0.55
11	8	30	1.75	2.94	0.51
12	13	30	1.75	2.92	0.51
13	3	30	1.75	3.26	0.57

$$D=-0.55+0.011v+0.532d+0.0056vd-0.001v^2-0.128d^2 \quad (14)$$

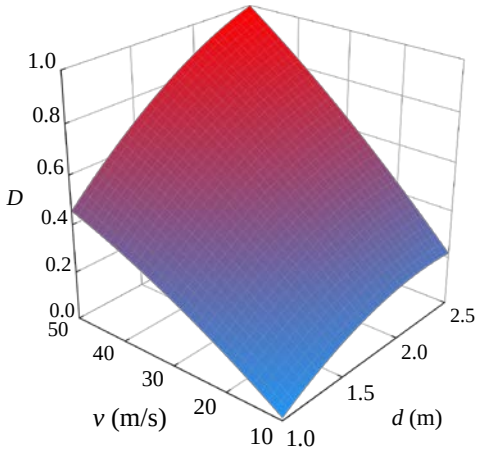

Figure 20. Response surface of the damage index under different impact velocities and rockfall diameter

The damage index of the HTWBP under rockfall impact is divided into four levels with 0.3, 0.6 and 0.9 as the critical value of damage respectively. Figure 21 shows the damage zoning diagram obtained according to Equation (14), where the ordinate is the rockfall diameter and the abscissa is the impact velocity of rockfall. As shown in the figure, three damage assessment curves divide the area into four parts: slight damage area

Preprints (www.preprints.org) | NOT PEER-REVIEWED | Posted: 20 September 2022 doi:10.20944/preprints202209.0274.v2

($D \le 0.3$), moderate damage area ($0.3 < D \le 0.6$), severe damage area ($0.6 < D \le 0.9$), and failure area ($D > 0.9$). With the damage zoning diagram, the fast assessment of the damage level of impacted HTWBP can be realized according to rockfall diameter and velocity after rockfall impact.

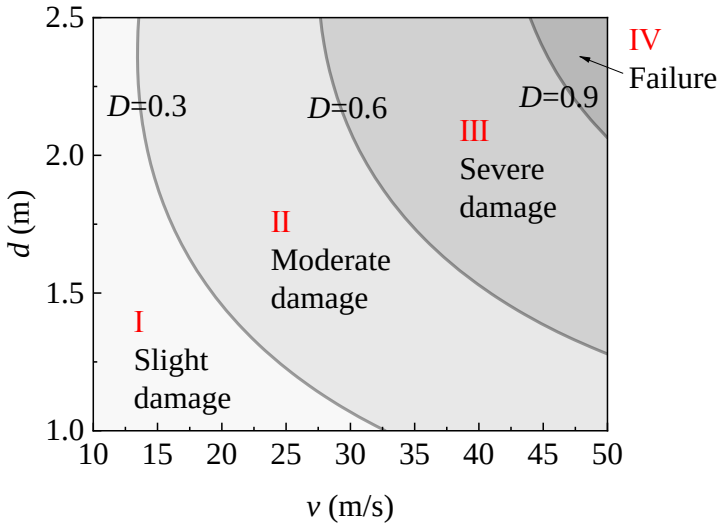

Figure 21. Damage zoning diagram

5 Discussion

In this research, the rockfall impact simulation is conducted against the HTWBP with the rockfall diameter ranging from 1.5 m-4.0 m and the rockfall velocity ranging from 10 m/s-30 m/s. The material parameters are obtained from the previous study of [1]. In Ref. [1], solid piers with circular and square cross-sections are impacted by the rockfall with diameters of 1.2 m, 1.5 m and 1.8 m, and velocities of 5 m/s, 10 m/s, 15 m/s and 20 m/s. To obtain a deeper insight into the rockfall-pier impact performance, the results of this study and Ref. [1] are compared here when the rockfall diameter is 1.5 m and velocity is 10 m/s. The peak impact force of this study and Ref. [1] is listed in Table 10.

The qualitative similarity between this study and Ref. [1] is: When the pier is impacted by a rockfall, the impact force shows an impulse characteristic, and the duration of the impulse load is approximately 0.01s. This similarity signals that the cross-section type does not influence the time-history characteristic of the impact force.

The quantitative similarity between this study and Ref. [1] is: As listed in Table 10, the difference in the peak impact force between this study and Ref. [1] is quite close (less than 10%), indicating that the simulation results of this research are credible. In addition, the similar results between this research and the literature may also imply that the biggest difference between an HTWBP and a solid pier is the damage and deformation characteristic.

Table 10. Comparison of the peak impact force between this study and Ref. [1].

Velocity (m/s)	Peak impact force (×10³ kN)			Difference (×10³ kN)
	Circular pier in Ref. [1]	Square pier in Ref. [1]	This research	
10	11.9	11.8	12.9	1.0~1.1

When heavy rainfalls, earthquakes and debris flows happen, a large number of rockfalls may impact the bridge in a short time. Therefore, Figure 22 compares the damage pattern of the HTWBP when impacted by a single rockfall and double rockfalls at

 doi:10.20944/preprints202209.0274.v2

the same time. In the single-rockfall case (C9), the rockfall diameter is 3.0 m and the impact height is 40 m. In the double-rockfall case, the impact height is 30 and 40 m. The other parameters of the two cases are the same. As shown in Figure 22, the elliptic damage area of the pier near the two rockfalls connects when impacted by two rockfalls. Compared with the single-rockfall case, the damage extent of the HTWBP in double-rockfall case is severer at the impact area and the pier bottom because the impact energy is higher.

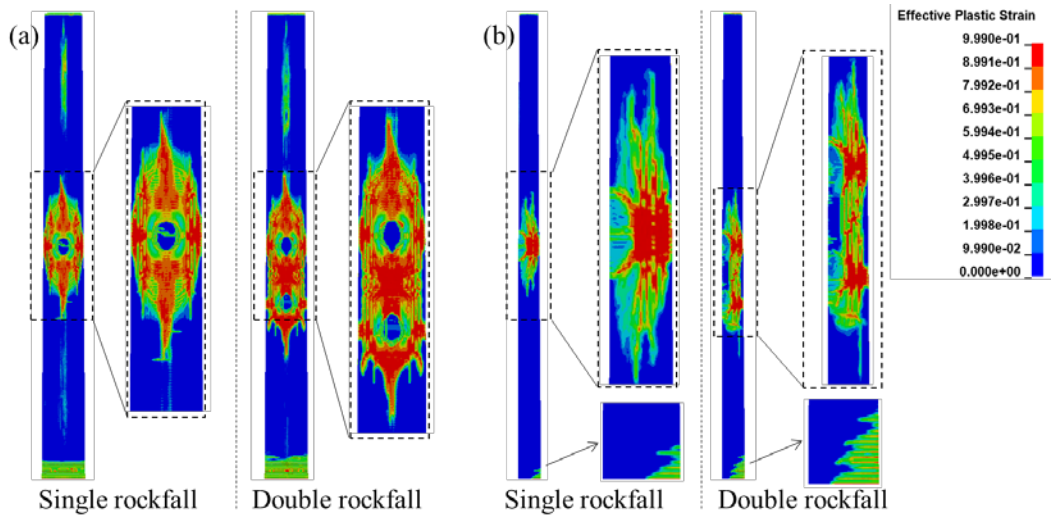

Figure 22. Comparison between single rockfall and double rockfalls impact: (a) Front view; (b) Side view.

6 Conclusion

In the current research, ANSYS/LS-DYNA is used to establish a high-precision rockfall-HTWBP model. The impact force, damage and dynamic response characteristics of HTWBP under the rockfall impact are studied. A damage assessment method with a damage zoning diagram based on the response surface method is established. The main conclusions are as follows:

1）The impact force of rockfall has a considerable impulse characteristic, and the duration of the impulse load is approximately 0.01s. When the impact position is closer to the pile cap, the pier is constrained more strongly and the corresponding peak impact force is larger. The peak impact force increases with the increase of impact velocity, rockfall diameter and concrete strength. When the concrete strength grade increases from 30 MPa to 50 MPa, the peak impact force only increases by approximately 5%.

2）The impacted surface is dominated by the final elliptic damage with the conical and strip damage areas as the symmetry axis. At the side surface, the damage develops from a triangular damage area into a radial damage area across the side surface of the pier. The cross-sectional damage mode is compression failure in the impact area and shear failure at the corner.

3)The displacement of the top and bottom of the pier is significantly lower than that of other cross-sections due to constraints. The time when the maximum displacement occurs of the cross-sections below the impact position is earlier than the cross-sections upper the impact position, because the upper part of the pier has greater flexibility and is more prone to deformation.

4）The maximum displacement occurs in the middle height of the pier. This is because the HTWBP has a smaller cross-section at the top and a larger cross-section at the bottom. The lower part of the pier has a larger stiffness and a stronger ability to resist deformation. The maximum displacement increases with impact height, impact velocity

and rockfall diameter and decreases with the uniaxial compressive strength of the concrete.

5）The initial impact velocity and diameter of the rockfall are the most remarkable parameters affecting the damage indices. The damage assessment method with a damage zoning diagram based on the response surface method is established. With the proposed damage assessment method with a damage zoning diagram, the fast assessment of the damage level of impacted HTWBP can be realized according to rockfall diameter and velocity after rockfall impact.

Limitation: The current simulation only considers four parameters. More relevant parameters should be considered in future research. In addition, when heavy rainfalls, earthquakes and debris flows happen, a large number of rockfalls may impact the bridge in a short time. Therefore, future research should consider multiple rockfalls impacting the bridge at the same time and in sequence.

Author Contributions: Conceptualization, Fei Li; Data curation, Fei Li; Formal analysis, Fei Li and Yikang Liu; Funding acquisition, Jian Yang; Investigation, Yikang Liu; Methodology, Fei Li; Writing – original draft, Yikang Liu; Writing – review & editing, Fei Li and Jian Yang.

Funding: This research was funded by the Hunan Natural Science Foundation, Chian (Project Grant No. 2018JJ2526) and the Natural Science Foundation of Science and Technology Planning Project of Gansu Province, China (Grant No. 20JR10RA132).

Conflicts of Interest: The authors declare no conflict of interest.

Reference:

1. Xie R.; Fan W.; Liu B.; Shen D. Dynamic behavior and vulnerability analysis of bridge columns with different cross-sectional shapes under rockfall impacts. *Structures.* **2020**, 26, 471-86, doi:10.1016/j.istruc.2020.04.042

2. Zhang X; Wang X; Chen W; Wen Z; Li X. Numerical study of rockfall impact on bridge piers and its effect on the safe operation of high-speed trains. *Structure and Infrastructure Engineering*. **2021**, 17(1): 1-19, doi: 10.1080/15732479.2020.1730406

3. Consolazio G.R.; Cook R.A.; McVay M.C.; Cowan D.; Biggs A.; Bui L. Barge impact testing of the St. George Island Causeway Bridge, Phase III: physical testing and data interpretation. **2006**.

4. Buth C.E.; Brackin M.S.; Williams W.F.; Fry G.T. Collision loads on bridge piers: phase 2, report of guidelines for designing bridge piers and abutments for vehicle collisions. *Texas Transportation Institute*; **2011**.

5. Zhang X.; Wang X.; Chen W.; Wen Z.; Li X. Numerical study of rockfall impact on bridge piers and its effect on the safe operation of high-speed trains. *Struct. Infrastruct. Eng.* **2021**, 17(1), 1-19, doi:10.1080/15732479.2020.1730406

6. He S.; Yan S.; Deng Y.; Liu W. Impact protection of bridge piers against rockfall. *Bull. Eng. Geol. Environ*. **2019**, 78(4), 2671-80, doi:10.1007/s10064-018-1250-5

7. Sun X.; Bi Y.; Zhou R.; Zhao H.; Fu X.-L.; Zhao P., et al. Experimental Study on the Damage of Bridge Pier under the Impact of Rockfall. *Adv. Civil Eng.* **2021**, 2021, doi:10.1155/2021/6610652

8. Bertrand D.; Kassem F.; Delhomme F.; Limam A. Reliability analysis of an RC member impacted by a rockfall using a nonlinear SDOF model. *Eng. Struct.* **2015**, 89, 93-102, doi:10.1016/j.engstruct.2015.01.051

9. Ventura A.; De Biagi V.; Chiaia B. Effects of rockfall on an elastic-plastic member: A novel compliance contact model and dynamic response. *Eng. Struct.* **2017**, 148, 126-44, doi:10.1016/j.engstruct.2017.06.046

10. Zhang X.; Wang X.Y.; Chen W.S.; Wen Z.P.; Li X.Z. Numerical study of rockfall impact on bridge piers and its effect on the safe operation of high-speed trains. *Struct. Infrastruct. Eng.* **2021**, 17(1), 1-19, doi:10.1080/15732479.2020.1730406

11. Deng L.; Wang F.; He W. Dynamic Impact Factors for Simply-Supported Bridges Due to Vehicle Braking. *Adv. Struct. Eng.* **2015**, 18(6), 791-801, doi:10.1260/1369-4332.18.6.791

12. Deng L.; Yan W.; Zhu Q. Vehicle Impact on the Deck Slab of Concrete Box-Girder Bridges due to Damaged Expansion Joints. *J. Bridge Eng.* **2016**, 21(2), doi:10.1061/(asce)be.1943-5592.0000796

13. Yu Y.; Deng L.; Wang W.; Cai C.S. Local impact analysis for deck slabs of prestressed concrete box-girder bridges subject to vehicle loading. *J. Vib. Control.* **2017**, 23(1), 31-45, doi:10.1177/1077546315575434

14. Do T.V.; Pham T.M.; Hao H. Proposed design procedure for reinforced concrete bridge columns subjected to vehicle collisions. *Structures.* **2019**, 22, 213-29, doi:10.1016/j.istruc.2019.08.011

15. Shi Y.; Hao H.; Li Z.-X. Numerical derivation of pressure-impulse diagrams for prediction of RC column damage to blast loads. *Int. J. Impact Eng.* **2008**, 35(11), 1213-27, doi:10.1016/j.ijimpeng.2007.09.001

16. Fan W.; Liu B.; Consolazio G.R. Residual Capacity of Axially Loaded Circular RC Columns after Lateral Low-Velocity Impact. *J. Struct. Eng.* **2019**, 145(6), doi:10.1061/(asce)st.1943-541x.0002324

17. Wang, Y.; Liang, S.; Huang, C.;Wang, R. Foundation Settlement Response of Existing High-Speed Railway Bridge Induced by Construction of Undercrossing Roads. *Sustainability* **2022**, 14, 8700. https://doi.org/10.3390/su14148700

18. Li, F.; Sun, R.; Zhang, Y.; Wang, G.; Xiang, G. Dynamic Response Characteristics and Damage Evolution of Multi-Layer Combined Coal and Rock Mass under Impact Loading. *Sustainability* **2022**, 14, 9175. https://doi.org/10.3390/su14159175

19. Li, P.; Li, T.; Lu, Z.; Li, J. Study on Dynamic Response of Novel Masonry Structures Impacted by Debris Flow. Sustainability **2017**, 9, 1122. https://doi.org/10.3390/su9071122

20. Tan, B. Experimental Study on Damage Evolution Characteristics of Concrete under Impact Load Based on EMI Method. *Sustainability* **2022**, 14, 10557. https://doi.org/10.3390/su141710557

21. Fujikake K.; Li B.; Soeun S. Impact Response of Reinforced Concrete Beam and Its Analytical Evaluation. *J. Struct. Eng.* **2009**, 135(8), 938-50, doi:10.1061/(asce)st.1943-541x.0000039

22. Meng, J.; Xu, Z.; Liu, Z.; Chen, S.; Wang, C.; Zhao, B.; Zhou, A. Experimental Study on the Mechanics and Impact Resistance of Multiphase Lightweight Aggregate Concrete. *Sustainability* **2022**, 14, 9606. doi:10.3390/su14159606

23. Fan W.; Xu X.; Zhang Z.; Shao X. Performance and sensitivity analysis of UHPFRC-strengthened bridge columns subjected to vehicle collisions. *Eng. Struct.* **2018**, 173, 251-68, doi:10.1016/j.engstruct.2018.06.113

24. Wang, S.; Xu, W.; Huang, X.; Yan, X.; Ma, J.; Sun, H.; Wang, J.; Chen, Y. Research on the Pounding Response and Pounding Effect of a Continuous Rigid-Frame Bridge with Fabricated Super-High Piers Connected by Grouting Sleeves. *Sustainability* **2022**, 14, 11334. doi:10.3390/su141811334

25. Zeng, X, Deng K, Wang Y, Yan G; Zhao C. Field Investigation and Numerical Analysis of Damage to a High-pier Long-span Continuous Rigid Frame Bridge in the 2008 Wenchuan Earthquake, *J. Earthqu. Eng.* **2021**, 26(10): 5204-5220. doi:10.1080/13632469.2020.1868361

26. Liu Y. The study of dynamic response and interaction mechanism of rock shed subject to rockfall impacting [M.A. dissertation]. Chengdu, China: Chengdu University of Technology; 2017. (in Chinese).

27. Xiao L. Research on the impact of mountain rolling stone on the pier and its reinforcement [M.A. dissertation] Chengdu, China: Southwest Jiaotong University; 2017. (in Chinese).

28. Zhang X; Hao H; Li C. Experimental investigation of the response of precast segmental columns subjected to impact loading. *Int. J. Impact Eng.* **2016**, 95: 105-124, doi:10.1016/j.ijimpeng.2016.05.005